THE JOURNAL OF PHYSICAL CHEMISTRY A
A JOURNAL OF THE AMERICAN CHEMICAL SOCIETY

pubs.acs.org/JPCA

Article

Ultrafast Dynamics of a Molecular Switch from Resonance Raman Spectroscopy: Comparing Visible and UV Excitation

Kristen H. Burns and Christopher G. Elles*

Cite This: J. Phys. Chem. A 2022, 126, 5932−5939

Read Online

ACCESS | Metrics & More | Article Recommendations | Supporting Information

ABSTRACT: Resonance Raman spectroscopy probes the ultrafast dynamics of a diarylethene (DAE) molecular switch following excitation into the first two optical absorption bands. Mode-specific resonance enhancements for Raman excitation at visible (750−560 nm) and near-UV (420−390 nm) wavelengths compared with the calculated and experimental off-resonance Raman spectrum at 785 nm reveal different Franck−Condon active vibrations for the two electronically excited states. The resonance enhancements at visible wavelengths are consistent with initial motion on the first excited-state that promotes the cycloreversion reaction, whereas the enhancements for excitation at near-UV wavelengths highlight motions involving conjugated backbone and phenyl ring stretching modes that are orthogonal to the reaction coordinate. The results support a mechanism involving rapid internal conversion from the higher-lying state followed by cycloreversion on the first excited state. These observations provide new information about the reactivity of DAE derivatives following excitation in the visible and near-UV.

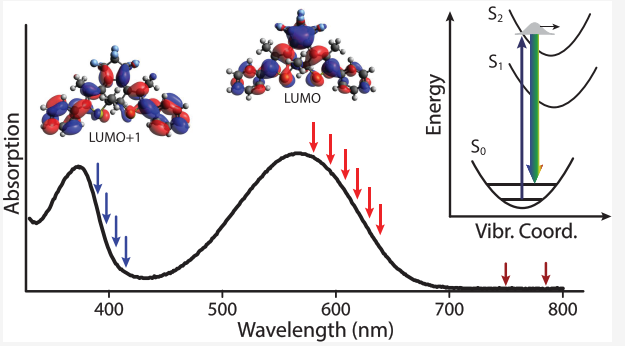

1. INTRODUCTION

Photochromic molecular switches undergo chemical reactions that result in a color change upon irradiation with light. These light-sensitive molecules have applications ranging from optogenetics[1−3] to solar energy harvesting[4,5] and optical data storage.[6−9] They have also been used as model compounds for studying the fundamental details of photochemical reactions, with the inherent spectral change providing a convenient way to monitor the transformation between different states of the molecule.[7] For example, many diarylethene-based photoswitches undergo reversible pericyclic reactions between a transparent open-ring isomer and a colorful closed-ring isomer when exposed to UV and visible light, respectively.[5,7,10−14] The two isomers often have very different electronic absorption spectra due to changes in π-conjugation along the backbone of the molecule upon photoswitching.

The molecule in Figure 1, which we label DAE throughout this paper, has been a popular target for both applied and fundamental studies due to favorable spectral characteristics and excellent fatigue-resistance.[7] Fatigue-resistance refers to the ability of the molecule to repeatedly switch without degrading. Notably, the closed-ring isomer (DAEc) has two strong absorption bands in the visible and near-UV region of the spectrum that are not present for the open-ring isomer (DAEo). The lower-energy absorption band centered near 560 nm represents $\pi \rightarrow \pi^*$ excitation involving delocalized orbitals spanning the backbone of the molecule, whereas the higher-energy transition centered near 380 nm represents a transition

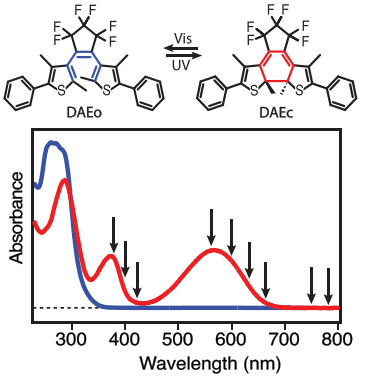

Figure 1. Absorption spectra of the open- and closed-ring isomers of DAE in cyclohexane. Arrows indicate the Raman excitation wavelengths.

that moves electron density from the central region of the molecule toward the peripheral phenyl rings.[11]

An interesting feature of DAE and many similar compounds is the relatively low quantum yield for cycloreversion. Although

Received: July 31, 2022
Revised: August 16, 2022
Published: August 26, 2022

https://doi.org/10.1021/acs.jpca.2c05435
J. Phys. Chem. A 2022, 126, 5932−5939

cyclization is very efficient, the ring-opening reaction for DAEc has a yield of only ~0.02 for one-photon excitation in the visible.[6,10,15−17] This low yield is convenient for recording the state of the molecule without inducing a change, but also inhibits conversion to the open-ring isomer. Excitation into higher-lying states provides a potential pathway for increasing the cycloreversion yield. However, direct excitation into either of the two lowest-lying excited states of DAEc results in cycloreversion with essentially the same quantum yield, suggesting that excitation to the higher-lying state from the equilibrium ground-state geometry results in rapid electronic relaxation from S_2 to S_1 prior to reaction on the S_1 potential energy surface.[18]

Aided by the distinct color change between the two isomers, many studies have examined the excited-state dynamics of diarylethenes in an attempt to gain new insights into the fundamental dynamics of cycloreversion reactions, including reactions involving the higher-lying states.[10,15,19−22] Most of the earlier studies explored the dynamics of DAEc using steady-state or time-resolved optical spectroscopy to probe changes in the molecule. While optical measurements are very sensitive to changes in the electronic state, they generally lack structural information. Therefore, the current study uses resonance Raman spectroscopy to probe the initial (sub-30 fs) dynamics of DAEc with vibrational specificity. Importantly, resonance Raman spectroscopy probes the dynamics in the Franck−Condon region of the excited state through mode-specific resonance enhancements of the Raman spectrum.[23−28] The vibrational spectrum reflects the equilibrium ground-state structure of the molecule, but mode-specific enhancements due to the electronic resonance condition reveal the relative degree of displacement of the upper-state potential energy surface along each of the ground-state vibrational normal modes. Modes with the greatest displacements in the electronically excited state have the strongest enhancements in the resonance Raman spectrum, thus reporting on the initial motions of the wave packet upon electronic excitation to the upper state.[23,26,29]

In this contribution, we report resonance Raman spectra with excitation wavelengths spanning the two lowest absorption bands of DAEc (indicated by the arrows in Figure 1). Changing the resonance condition reveals different mode-specific enhancements for the two absorption bands, and therefore indicates distinct dynamics in the Franck−Condon region of the two excited states. We compare the experimental spectra with the calculated (off-resonance) spectrum in order to assign the observed transitions, then interpret the resonance Raman spectra in terms of the initial motions in each of the excited states. The different resonance enhancements for the two absorption bands provide evidence for a direct reaction channel on the S_1 potential energy surface, whereas excitation to S_2 results in initial wave packet motion along a coordinate that facilitates rapid relaxation to S_1.

2. EXPERIMENTAL SECTION

We measured the Raman spectrum of DAEc using spontaneous Raman scattering at 785 nm and stimulated Raman scattering at various other wavelengths ranging from 750 to 390 nm. Stimulated Raman scattering allows time-gating of the Raman signal and therefore prevents interference from fluorescence and other background signals resulting from resonant excitation.[30−32] The samples consist of 20, 5, 3, and 0.3 mM solutions of DAE in cyclohexane for the measurements at 785, 750, 390−420, and 560−660 nm, respectively. We obtain DAE [1,2-bis(2,4-dimethyl-5-phenyl-3-thienyl) perfluorocyclopentene] from TCI America in the open-ring isomer and dissolve it in spectroscopic grade cyclohexane (Fisher Scientific). We irradiate each sample solution with a 310 nm LED for several hours in order to reach a photostationary state (PSS) consisting of primarily the closed-ring isomer.[16] Residual DAEo would not contribute appreciably to the Raman signal even in higher concentration, due to the off-resonance excitation and weaker overall Raman activity (see the Supporting Information).[18,33]

For the stimulated Raman measurements, we use a gear pump to flow the sample solution through a cell with 0.5 mm path length and 1-mm-thick CaF_2 windows. Flowing the sample prevents accumulation of photoproduct in the laser focal volume due to resonant excitation of DAEc. We also continuously irradiate the sample reservoir with a 310 nm LED in order to maintain PSS of the recirculating sample solution over several hours of laser excitation. Optical absorption spectra measured before and after each experiment show that the relative concentration of closed- and open-ring isomers does not change throughout the duration of the experiment, and we observe no evidence of photodamage.

Stimulated Raman spectra were measured using the output of an amplified Ti:sapphire laser (Coherent, Legend Elite HP, 1 kHz, 35 fs). A portion of the output pumps an optical parametric amplifier (OPA) with one or two additional stages of second harmonic generation (SHG) to provide the tunable Raman pump pulses. The final stage of SHG generally uses a 25-mm-long BBO crystal (cut at 27.6° for 350−520 nm, or 21.1° for 500−650 nm) for spectral compression,[34] followed by a 4*f* spatial filter that improves the spectral profile and further reduces the bandwidth to ~15 cm^{-1}.[35] In the case of 750 nm Raman pump pulses, we use a 2 mm crystal for SHG before passing through the spatial filter. In all cases, a variable neutral density filter attenuates the Raman pump pulses to 1.00 ± 0.05 μJ before focusing into the sample where they intersect the probe beam.

Focusing a small portion of the laser fundamental into a circularly translating CaF_2 disk produces fs broadband probe pulses via white-light continuum generation. Both pump and probe beams have vertical polarization and remain parallel to the plane of the laser table before overlapping in the sample at a small angle. We measure the stimulated Raman spectrum in the Stokes field for all excitation wavelengths except 750 nm, for which we use the anti-Stokes field in order to avoid spectral overlap with the laser fundamental. After the sample, the probe beam passes into a 1/4 m imaging spectrograph (Newport, MS260i) where a grating with a blaze angle matching the Raman pump and white-light probe range (1800 line/mm for 560−750 nm and 2400 line/mm for 390−420 nm) disperses the probe light onto a 2068-pixel linear CCD array (Hamamatsu, S11156−2048). Using a 50 μm entry slit on the spectrograph provides an instrument-limited spectral resolution of ~10 cm^{-1}, which covers about 10 pixels and is slightly better than the bandwidth of the Raman pump pulses. The probe light is measured on the CCD at the full 1 kHz repetition rate and the Raman pump is chopped at 500 Hz for shot-to-shot averaging and background subtraction. The resulting spectra are averaged over 4×10^5 laser shots at each excitation wavelength. Baseline correction methods are described in the Supporting Information.

https://doi.org/10.1021/acs.jpca.2c05435
J. Phys. Chem. A 2022, 126, 5932−5939

We record the spontaneous Raman spectrum of DAE at 785 nm using a commercial Raman spectrometer with 4 cm^{-1} resolution (Ramulaser-785 laser source and Raman-HR-TEC-X2 spectrometer, Stellarnet). For this measurement, the sample is in a 1 cm quartz cuvette and is not irradiated with the UV LED during the experiment due to off-resonance excitation. We average for approximately 10 min with minimal photoconversion.

For comparison with the experimental results, we calculate the off-resonance Raman spectrum of DAEc using density functional theory (DFT) with B3LYP/aug-cc-pVDZ. We use the Gaussian 03 software package[36] to find the optimized geometry and normal mode coordinates, then convert the calculated Raman activities to intensities.[37] While no resonance condition was included in the calculation, the resonance enhancement only affects the magnitude of the Raman intensities, not the frequencies. We apply a frequency scaling factor[38] of 0.970 and include 15 cm^{-1} broadening of each transition in order to aid the comparison with experiment. Previous work suggests good agreement between experimental and calculated frequencies at this level of theory.[29,39−41]

3. RESULTS

Figure 2 illustrates the wavelength dependence of the resonance Raman spectrum of DAEc by comparing the calculated off-resonance spectrum with the experimental results for various resonance conditions. The experimental results include the spontaneous Raman spectrum at 785 nm and stimulated Raman spectra at 750, 600, and 390 nm. The figure also shows the solvent spectrum of cyclohexane, which has been subtracted from each of the experimental spectra.

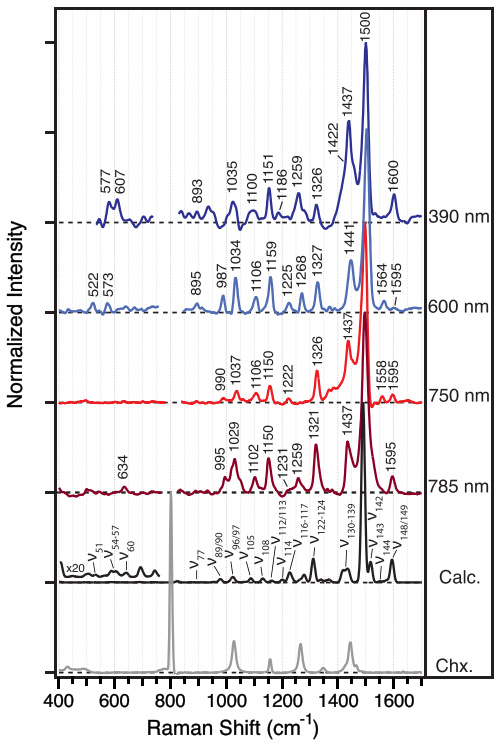

Figure 2. Raman spectrum of DAEc at four different excitation wavelengths and the calculated off-resonance Raman spectrum (including 0.970 frequency scaling and 15 cm^{-1} broadening). The spectrum of the cyclohexane solvent is included for reference.

Several of the most prominent Raman bands for DAEc have been indicated in the figure and are listed in Table 1, along with mode assignments from comparison with the calculations.[40] The table shows experimental frequencies from the 785, 600, and 390 nm spectra; small differences between the reported values may reflect solvent subtraction and baseline correction errors. The table only includes calculated transitions with appreciable intensity, and we combine nearly degenerate modes (less than 1−2 cm^{-1} spacing) that have closely related vibrational displacements. These combined modes are typically symmetric and antisymmetric combinations of the vibrations on the peripheral phenyl rings that we label as $\nu_{a/b}$. A complete table of calculated frequencies and intensities for DAEc is available in the Supporting Information.

All of the spectra in Figure 2 have been normalized to the most intense transition near 1500 cm^{-1} in order to facilitate comparison of the relative intensities. There are many Raman bands in the experimental spectrum at 785 nm that are also evident at other wavelengths, including the prominent transitions near 1437, 1321, 1150, and 1029 cm^{-1}. However, closer inspection of Figure 2 reveals additional bands that have appreciable intensity only in the resonance-enhanced spectra, including the bands near 1564, 1268, 1225, and 522 cm^{-1} in the 600 nm spectrum, as well as the shoulder near 1422 cm^{-1} and the bands near 1186, 607, and 577 cm^{-1} in the 390 nm spectrum.

The Raman gain profiles that we measure by tuning the excitation wavelength into resonance with each of the optical absorption bands of DAEc highlight the mode-specific resonance enhancements. For example, Figure 3 shows the progression of Raman spectra across the range 785−560 nm, which covers the low-energy side of the first electronic absorption band. The Raman pump was only tuned over the lower-energy side of the absorption band to avoid dispersive line shapes[42,43] and to minimize absorption of the probe light by the sample. The spectra were normalized to the 800 cm^{-1} mode of cyclohexane before solvent subtraction in order to account for any changes in focal conditions or spatial overlap of the pump and probe beams at the different Raman excitation wavelengths. The figure highlights the overall increase of the Raman intensity as the excitation wavelength is tuned into resonance with the electronic absorption at 560 nm.

In order to emphasize the mode-specific resonance enhancements, Figure 4 tracks the Raman gain profiles for each of the prominent vibrations listed in Table 1. Here, the intensities for each mode have been normalized to the intensity in the 785 nm spectrum, the most off-resonance measurement, in order to show changes in the relative gain independent of the absolute intensity. We separate the modes into two subsets in the figure based on the relative behavior compared with the profile of the absorption spectrum (solid line in the figure). The first set, Figure 4A, includes bands with Raman gain profiles that grow more slowly than the absorption band with decreasing wavelength (e.g., 1497, 1441, 1327, 1159, 1106, and 1034 cm^{-1}). These modes generally have significant off-resonance intensity and are mainly assigned as backbone deformation and ring breathing modes. In contrast, Figure 4B shows a set of Raman bands with gain profiles that increase much more rapidly than the electronic absorption profile (1564, 1225, 895, 573, 522 cm^{-1}). These modes are often indistinguishable from noise in the off-resonance spectrum at 785 nm, but rapidly gain intensity as the excitation wavelength tunes into resonance

https://doi.org/10.1021/acs.jpca.2c05435
J. Phys. Chem. A 2022, 126, 5932−5939

Table 1. Raman Band Assignments for DAEc

Experiment (cm^{-1})			Calculated[a]			
785 nm	600 nm	390 nm	Freq (cm^{-1})	Mode	Intensity (Å^4/amu)	Mode Assignment[b]
-	522	-	526	ν_{51}	47	Ring deformation of thiophenes and CHD
-	573	577	570	ν_{54}	10	Ring deformation of all rings
-	-	-	582	ν_{55}	91	Out-of-plane backbone str.
-	-	607	601	ν_{57}	63	Central ring breathing
634	-	-	627	ν_{60}	32	Ring deformation of thiophenes and CHD
-	895	893	873	ν_{77}	52	C−C str. between reactive carbons
-	-	-	954	$\nu_{83/84}$	76	Out-of-plane CH wag on phenyls
995	987	-	978	$\nu_{89/90}$	665	Phenyl ring breathing
-	-	-	1012	ν_{92}	146	Methyl umbrella
-	-	-	1015	$\nu_{93/94}$	69	Phenyl ring breathing and CH wag
1029	1034	1035	1022	$\nu_{96/97}$	1191	Phenyl CH wag
-	-	-	1030	ν_{98}	64	CHD ring breathing, methyl CH wag
-	-	-	1035	ν_{99}	107	Deloc. backbone str., methyl umbrella
1102	1106	1100	1087	ν_{105}	591	CHD ring breathing, methyl str.
1150	1159	1151	1129	ν_{108}	873	C−C str. in CHD ring and methyl
-	-	1186	1161	$\nu_{112/113}$	429	Phenyl CH bend
-	1225	-	1199	ν_{114}	516	C−C str. in CHD ring
1231	-	-	1225	ν_{116}	1933	Delocalized backbone str. (sym.)
1259	-	1259	1234	ν_{117}	500	Delocalized backbone str. (antisym.)
-	1268	-	1262	ν_{118}	474	C−C str. of central rings
-	-	-	1277	ν_{119}	1490	C−C str. in phenyl, CH wag
-	-	-	1309	$\nu_{122/123}$	1745	Phenyl CH wag, low amp backbone str.
1321	1327	1326	1312	ν_{124}	3106	Delocalized backbone stretching
-	-	-	1338	ν_{125}	464	C=C str. in thiophene and CHD
-	-	-	1353	ν_{126}	167	Methyl CH umbrella
-	-	-	1358	ν_{127}	116	Methyl CH umbrella
-	-	-	1368	$\nu_{128/129}$	456	Methyl CH umbrella; methyl C−C str.
-	-	1422	1415	$\nu_{130/131}$	1929	Localized C−C phenyl ring str. and CH wag
1437	1441	1437	1424−40	$\nu_{132-139}$	3146	Methyl CH bend and umbrella (mixed)
1500	1497	1500	1490	ν_{142}	31212	C=C backbone str., methyl umbrella
-	-	-	1515	ν_{143}	3715	C=C backbone str., phenyl CH wag
-	1564	-	1550	ν_{144}	335	Deloc. C=C backbone str.; higher amp. in CHD
-	-	-	1564	ν_{145}	75	Localized phenyl C−C str.
-	-	-	1574	ν_{147}	528	C=C str. in CHD
1595	1595	1600	1592	$\nu_{148/149}$	3654	Localized C=C phenyl ring str.

[a]B3LYP/aug-cc-pVDZ with 0.970 frequency scaling factor.[38] Includes only modes with intensity >50 Å^4/amu or that involved in assignments. Nearly degenerate modes with <1 cm^{-1} spacing and similar vibrational displacements are combined. [b]CHD = cyclohexadiene.

with the absorption band. Notably, all of the modes with rapidly increasing gain profiles involve significant stretching of the central ring structure of the molecule, including the cyclohexadiene ring where the C−C bond breaking occurs during the cycloreversion reaction.

Similarly, Figure 5 shows the progression of Raman spectra when the excitation wavelength is tuned into resonance with the near-UV transition of DAEc. In this case, the Stokes probe field partially overlaps the absorption band at longer wavelengths, limiting the Raman excitation to 420 nm and below. The mode-specific enhancements in this range are highlighted in Figure 6, where the gain profile at each frequency is normalized to the off-resonance intensities. Normalization using the intensities from the 785 nm Raman spectrum results in gain profiles that consistently fall below the normalized absorption spectrum in the near-UV; therefore we also multiply all of the Raman gain profiles in this wavelength range by a factor of 10 to compensate for the $\sim\nu^4$ excitation-frequency dependence of the off-resonance Raman scattering in the cyclohexane reference spectrum. Interestingly, the modes with the most aggressive gain profiles at this wavelength are all relatively low frequency (893, 607, and 577 cm^{-1}), consistent with our earlier observation that lower-frequency modes of aryl-substituted thiophenes tend to be more sensitive to resonance enhancement effects than the higher-frequency modes.[29,37] We also identify several bands (near 1600, 1437, and 1259 cm^{-1}) with slightly elevated Raman gain profiles compared with the others. The assigned modes involve vibrations that are mostly located outside of the central region of the molecule, with the enhancement of the shoulder near 1422 cm^{-1} and the band near 1186 cm^{-1} in the 390 nm spectrum pointing to significant stretching and distortion of the phenyl rings on the ends of the molecule.

4. DISCUSSION

Mode-specific resonance Raman enhancements probe the ultrafast dynamics following excitation into each of two lowest absorption bands of DAEc. The different enhancements for resonance with the two absorption bands provide new insight into the initial dynamics in the Franck−Condon region and helps explain why excitation to the higher-lying state does not increase the cycloreversion reaction yield even though the total

https://doi.org/10.1021/acs.jpca.2c05435
J. Phys. Chem. A 2022, 126, 5932−5939

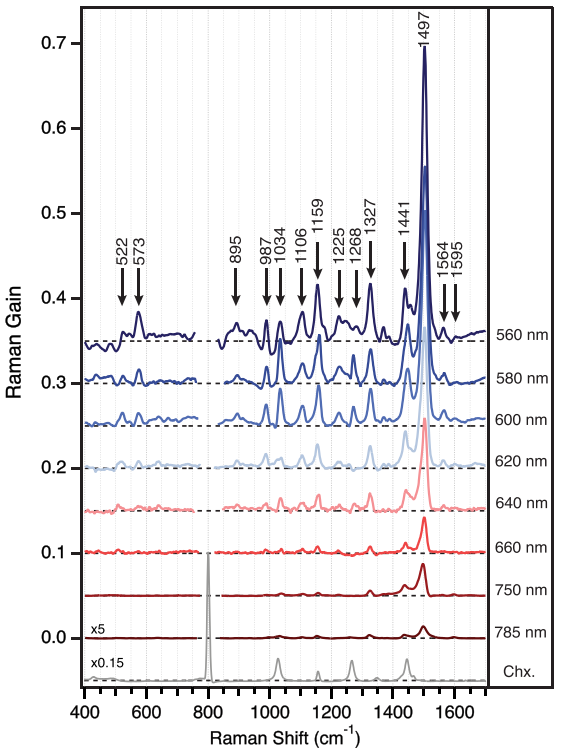

Figure 3. Variation of the Raman spectrum of DAEc for excitation wavelengths across the first absorption band (785 to 560 nm). The solvent spectrum is shown for comparison.

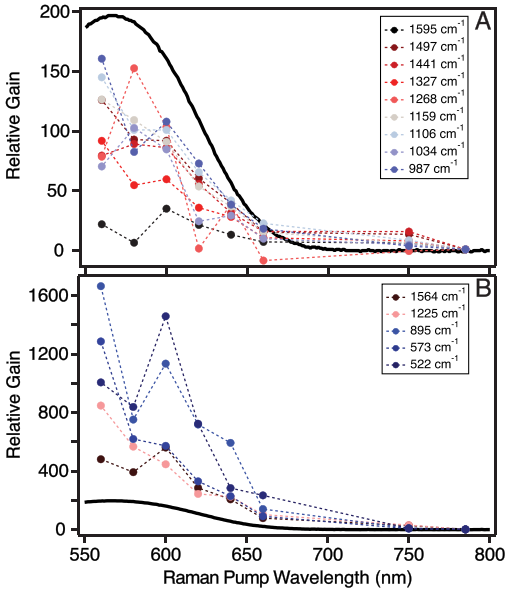

Figure 4. Raman gain profiles in the 560−785 nm wavelength range. The solid black line is the intensity profile for the ground-state absorption spectrum. All curves are normalized to the intensity at 785 nm.

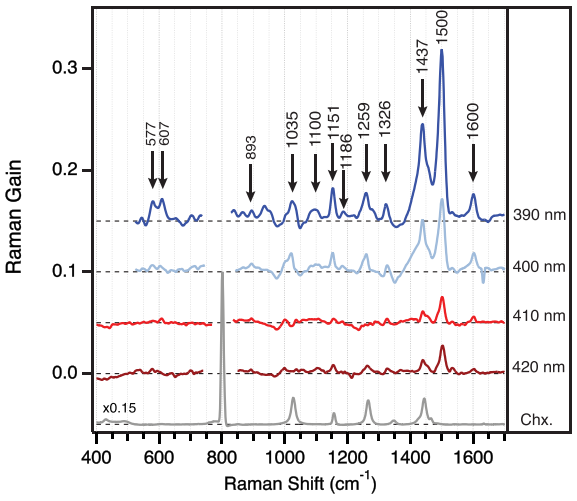

Figure 5. Variation of the Raman spectrum of DAEc for excitation wavelengths across the second absorption band (420 to 390 nm). The solvent spectrum is shown for comparison.

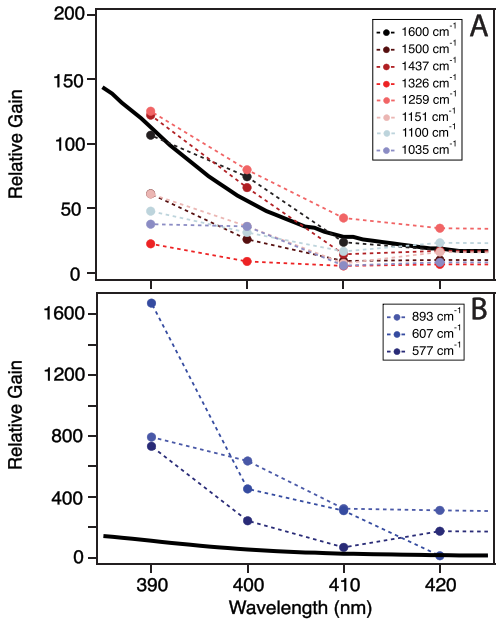

Figure 6. Raman gain profiles in the 390−420 nm wavelength range. The solid black line is the intensity profile for the ground-state absorption spectrum. All curves are normalized to the intensity at 785 nm then multiplied by a factor of 10 to account for the $\sim\nu^4$ excitation dependence of the solvent reference spectrum.

excitation energy at 380 nm is more than 50% higher than at 560 nm. Previous pump−probe experiments suggested that the higher-lying state relaxes within ∼200 fs and then follows essentially the same reaction pathway that is observed for direct excitation to the lower-lying state,[18] but could not provide quantitative information about the relaxation mechanism beyond the lifetime. While some differences could be predicted *a priori* on the basis of the different electronic character of the two transitions (see Figure 7), the Raman intensities give a more quantitative description of the upper-state potential energy surfaces and the initial dynamics along them.

In particular, we observe enhancements of vibrational modes that map onto the reactive and nonreactive pathways for excitation into the first and second absorption bands, respectively. Key differences are highlighted in the characteristic behavior of the modes above ∼1500 cm^{-1}, where the low density of vibrational states simplifies the mode assignments. For example, the band near 1564 cm^{-1} is significantly enhanced for excitation into the first absorption band and is assigned as ν_{144}, a delocalized C═C stretching mode that has

https://doi.org/10.1021/acs.jpca.2c05435
J. Phys. Chem. A 2022, 126, 5932−5939

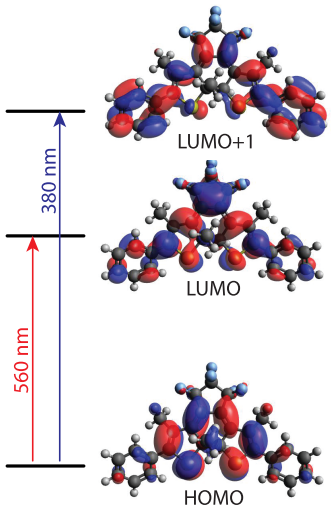

Figure 7. Representation of the highest occupied (HOMO) and two lowest unoccupied molecular orbitals (LUMO) of DAEc. Optical transitions in the visible and near-UV regions of the spectrum are dominated by the indicated excitations. Excitation in the visible is largely localized within the central ring structure of the molecule, whereas excitation in the near-UV moves charge density into the peripheral phenyl rings.

significant displacement in the central thiophene and cyclohexadiene rings of DAEc. Enhancement of this mode reflects the delocalized $\pi\pi^*$ character of the excited state being most pronounced in the planar (core) region of the molecule. Interestingly, the vibration associated with ν_{144} has some character that resembles the cycloreversion reaction coordinate because it involves stretching of the C−C bond that ultimately breaks in order to reach the open-ring isomer product state. While the bond-breaking does not happen immediately upon excitation, there is growing consensus that a barrier crossing along this C−C bond-stretching coordinate is a crucial step in the early dynamics.[12,18,44−46] Apparently, excitation to the visible absorption band at least partially excites this motion, although the ∼3 ps time scale from prior transient absorption measurements indicates more complicated dynamics outside of the Franck−Condon region.

In contrast, excitation in the near-UV results in resonance enhancement of a Raman band near 1600 cm^{-1} that we assign as $\nu_{148/149}$, a pair of localized phenyl ring stretching modes located on the periphery of the molecule. This vibration is largely isolated from the central ring structure, and therefore suggests that the initial dynamics following excitation to the near-UV band does not map directly onto the reaction coordinate. Instead, the enhancement of predominantly phenyl-stretching modes throughout the near-UV resonance Raman spectrum reflects the charge-transfer character of the transition that moves electron density to the peripheral phenyl rings. While $\nu_{148/149}$ is also observed in the off-resonance spectrum (i.e., the calculated and 785 nm spectra) due to the large change in polarizability along this coordinate, the Raman gain profile in Figure 6 reveals additional resonance enhancement for this mode compared with many others. Additionally, the slightly lower frequencies in the 785−560 nm spectra may reflect contributions from a nearby C═C stretching mode of the cyclohexadiene ring, ν_{147}, for visible excitation wavelengths.

We observe similar wavelength-dependent differences in the resonance enhancements of other modes, as well, including the enhancements of $\nu_{112/113}$ and ν_{114} (the 1186 and 1225 cm^{-1} bands, respectively). The former is enhanced primarily in resonance with the near-UV absorption and is assigned as a pair of phenyl C−H bending modes, whereas ν_{114} is a C−C stretching and methyl bending mode that has significant amplitude in the cyclohexadiene ring and is only enhanced with visible excitation. As before, the phenyl modes are isolated from the reactive region of the molecule, but the C−C stretching motion of ν_{114} directly resembles the cycloreversion reaction coordinate due to the stretching within the cyclohexadiene ring and even the distortion of the methyl groups attached to the reactive carbon atoms, which we associate with rehybridization. In other words, the initial motion following excitation into the near-UV absorption band is orthogonal to the reaction coordinate, and therefore directs vibrational energy in a nonproductive motion, but excitation to the visible band populates vibrations that are likely to promote cycloreversion. While resonance Raman spectroscopy only probes the initial ∼30 fs of the wave packet motion, this observation may help explain why excitation to the higher-lying state does not increase the reaction yield compared with direct excitation to the first excited state. The dynamics on the S_1 surface spans a time scale of several picoseconds, but the very rapid (<200 fs) internal conversion from the higher-lying state after excitation in the near-UV depends largely on the initial wave packet motions that are probed by resonance Raman.

More detailed analysis of the resonance Raman enhancements may provide deeper insight into the excited-state dynamics of DAEc, including the different behaviors following excitation in the visible and near-UV. Previous resonance Raman studies of cyclohexadiene and other model compounds showed similar enhancement of vibrational modes related to the ring-opening reaction that we observe here following excitation at visible wavelengths.[47−52] Whereas the assignments in the earlier cases were often relatively straightforward based on the lower density of vibrational states for smaller molecules, challenges in assigning the vibrations and identifying unique vibrational motions associated with the resonance enhancements prevents a more explicit determination of the excited-state dynamics of DAEc at present. For example, it remains challenging to map the complex normal modes of DAEc onto specific reaction and relaxation coordinates. Nevertheless, the comparison of the resonance Raman spectra in the visible and near-UV provides unique insight that has no parallel in the earlier studies of smaller molecules where only a single excited state was accessible. More detailed calculations may provide the necessary framework for relating the ground-state vibrational normal modes to the cycloreversion reaction coordinate for this complex molecule.

5. CONCLUSION

We have reported resonance Raman spectra for a diarylethene photoswitch at 12 different Raman pump wavelengths. Overall, when the resonance condition is tuned to the lower-energy absorption band there are strong resonance enhancements of modes assigned to the central ring structure. These modes indicate that the primary motion of a wave packet on the first excited state initially involves deformation of the central cyclohexadiene ring, including C−C stretching that resembles the cycloreversion reaction coordinate. The enhancements of these specific motions suggests that excitation to this state initiates motion along a coordinate that could promote the ring

https://doi.org/10.1021/acs.jpca.2c05435
J. Phys. Chem. A 2022, 126, 5932−5939

opening reaction. In contrast, tuning the excitation to a higher-energy transition in the near-UV reveals enhancement of vibrational modes with displacement in the peripheral phenyl rings. The enhancements of phenyl modes suggest that the primary motions along this higher-lying state map onto modes that are orthogonal to the reaction coordinate. Instead, the initial motion in the phenyl rings may drive rapid electronic relaxation via internal conversion from S_n to S_1. While the initial assignments based on comparison of the experimental results with the calculated off-resonance Raman spectrum of DAEc highlights differences between the two electronic absorption bands, more detailed calculations are necessary in order to interpret the resonance enhancements in terms of specific reaction and relaxation pathways of DAEc.

■ ASSOCIATED CONTENT

Supporting Information

The Supporting Information is available free of charge at https://pubs.acs.org/doi/10.1021/acs.jpca.2c05435.

Comparison of resonance Raman spectra of DAEc and DAEo at three excitation wavelengths, description of the baseline correction method, comparison of calculated and experimental Raman spectra in the 800−1700 cm^{-1} range, coordinates for the optimized geometry of DAEc, table of calculated frequencies and intensities (PDF)

■ AUTHOR INFORMATION

Corresponding Author

Christopher G. Elles − *Department of Chemistry, University of Kansas, Lawrence, Kansas 66045, United States;* orcid.org/0000-0002-1408-8360; Email: elles@ku.edu

Author

Kristen H. Burns − *Department of Chemistry, University of Kansas, Lawrence, Kansas 66045, United States*

Complete contact information is available at: https://pubs.acs.org/10.1021/acs.jpca.2c05435

Notes

The authors declare no competing financial interest.

■ ACKNOWLEDGMENTS

This work was supported by the National Science Foundation (NSF) through grant CHE-1956387. The authors appreciate many valuable conversations with Prof. Marco Caricato and Dr. Matthew Barclay related to interpretation of computational Raman spectra, as well as contributions to the interpretation of the off-resonance Raman spectrum of DAE by undergraduate student Jessica Bair. CGE acknowledges support from the Individual Research and Development (IR/D) program while serving as a program director at NSF.

■ REFERENCES

(1) Cheng, H. B.; Qiao, B.; Li, H.; Cao, J.; Luo, Y.; Kotraiah Swamy, K. M.; Zhao, J.; Wang, Z.; Lee, J. Y.; Liang, X. J.; et al. Protein-Activatable Diarylethene Monomer as a Smart Trigger of Noninvasive Control over Reversible Generation of Singlet Oxygen: A Facile, Switchable, Theranostic Strategy for Photodynamic-Immunotherapy. *J. Am. Chem. Soc.* **2021**, *143*, 2413−2422.

(2) Fukushima, T.; Tamaki, K.; Isobe, A.; Hirose, T.; Shimizu, N.; Takagi, H.; Haruki, R.; Adachi, S. I.; Hollamby, M. J.; Yagai, S. Diarylethene-Powered Light-Induced Folding of Supramolecular Polymers. *J. Am. Chem. Soc.* **2021**, *143*, 5845−5854.

(3) Cahová, H.; Jäschke, A. Nucleoside-based diarylethene photoswitches and their facile incorporation into photoswitchable DNA. *Angewandte Chemie - International Edition* **2013**, *52*, 3186−3190.

(4) Sun, C. L.; Wang, C.; Boulatov, R. Applications of Photoswitches in the Storage of Solar Energy. *ChemPhotoChem.* **2019**, *3*, 268−283.

(5) Irie, M.; Fukaminato, T.; Matsuda, K.; Kobatake, S. Photochromism of diarylethene molecules and crystals: Memories, switches, and actuators. *Chem. Rev.* **2014**, *114*, 12174−12277.

(6) Shinoda, K.; Yokojima, S.; Fukaminato, T.; Nakamura, S. Determining Factor of the Quantum Yield of the Cyclization Reaction via Triplet States for Dye-Attached Diarylethene. *J. Phys. Chem. A* **2021**, *125*, 5895−5902.

(7) Irie, M. Diarylethenes for Memories and Switches. *Chem. Rev.* **2000**, *100*, 1685−1716.

(8) Tian, H.; Feng, Y. Next step of photochromic switches? *J. Mater. Chem.* **2008**, *18*, 1617−1622.

(9) Feringa, B. L. The Art of Building Small: From Molecular Switches to Motors (Nobel Lecture). *Angewandte Chemie - International Edition* **2017**, *56*, 11060−11078.

(10) Ishibashi, Y.; Okuno, K.; Ota, C.; Umesato, T.; Katayama, T.; Murakami, M.; Kobatake, S.; Irie, M.; Miyasaka, H. Multiphoton-gated cycloreversion reactions of photochromic diarylethene derivatives with low reaction yields upon one-photon visible excitation. *Photochemical and Photobiological Sciences* **2010**, *9*, 172−180.

(11) Matsuda, K.; Irie, M. Diarylethene as a photoswitching unit. *Journal of Photochemistry and Photobiology C: Photochemistry Reviews* **2004**, *5*, 169−182.

(12) Arruda, B. C.; Sension, R. J. Ultrafast polyene dynamics: The ring opening of 1,3-cyclohexadiene derivatives. *Phys. Chem. Chem. Phys.* **2014**, *16*, 4439−4455.

(13) Honick, C. R.; Peters, G. M.; Young, J. D.; Tovar, J. D.; Bragg, A. E. Core structure dependence of cycloreversion dynamics in diarylethene analogs. *Phys. Chem. Chem. Phys.* **2020**, *22*, 3314−3328.

(14) Irie, M.; Mohri, M. Thermally Irreversible Photochromic Systems. Reversible Photocyclization of Diarylethene Derivatives. *J. Org. Chem.* **1988**, *53*, 803−808.

(15) Miyasaka, H.; Murakami, M.; Okada, T.; Nagata, Y.; Itaya, A.; Kobatake, S.; Irie, M. Picosecond and femtosecond laser photolysis studies of a photochronic diarylethene derivative: Multiphoton gated reaction. *Chem. Phys. Lett.* **2003**, *371*, 40−48.

(16) Sotome, H.; Nagasaka, T.; Une, K.; Morikawa, S.; Katayama, T.; Kobatake, S.; Irie, M.; Miyasaka, H. Cycloreversion Reaction of a Diarylethene Derivative at Higher Excited States Attained by Two-Color, Two-Photon Femtosecond Pulsed Excitation. *J. Am. Chem. Soc.* **2017**, *139*, 17159−17167.

(17) Sotome, H.; Okajima, H.; Nagasaka, T.; Tachii, Y.; Sakamoto, A.; Kobatake, S.; Irie, M.; Miyasaka, H. Geometrical Evolution and Formation of the Photoproduct in the Cycloreversion Reaction of a Diarylethene Derivative Probed by Vibrational Spectroscopy. *ChemPhysChem* **2020**, *21*, 1524−1530.

(18) Ward, C. L.; Elles, C. G. Cycloreversion dynamics of a photochromic molecular switch via one-photon and sequential two-photon excitation. *J. Phys. Chem. A* **2014**, *118*, 10011−10019.

(19) Nagasaka, T.; Kunishi, T.; Sotome, H.; Koga, M.; Morimoto, M.; Irie, M.; Miyasaka, H. Multiphoton-gated cycloreversion reaction of a fluorescent diarylethene derivative as revealed by transient absorption spectroscopy. *Phys. Chem. Chem. Phys.* **2018**, *20*, 19776−19783.

(20) Tani, K.; Ishibashi, Y.; Miyasaka, H.; Kobatake, S.; Irie, M. Dynamics of cyclization, cycloreversion, and multiphoton-gated reaction of a photochromic diarylethene derivative in crystalline phase. *J. Phys. Chem. C* **2008**, *112*, 11150−11157.

(21) Ward, C. L.; Elles, C. G. Controlling the excited-state reaction dynamics of a photochromic molecular switch with sequential two-photon excitation. *J. Phys. Chem. Lett.* **2012**, *3*, 2995−3000.

(22) Miyasaka, H.; Murakami, M.; Itaya, A.; Guillaumont, D.; Nakamura, S.; Irie, M. Multiphoton gated photochromic reaction in a diarylethene derivative [11]. *J. Am. Chem. Soc.* **2001**, *123*, 753−754.

(23) Myers, A. B. 'Time-dependent' resonance Raman theory. *J. Raman Spectrosc.* **1997**, *28*, 389−401.
(24) Lee, S. Y.; Heller, E. J. Time-dependent theory of Raman scattering. *J. Chem. Phys.* **1979**, *71*, 4777−4788.
(25) Heller, E. J.; Sundberg, R. L.; Tannor, D. Simple aspects of raman scattering. *J. Phys. Chem.* **1982**, *86*, 1822−1833.
(26) Shin, K. s. K.; Zink, J. I. Quantitative Evaluation of the Relationships between Excited-State Geometry and the Intensities of Fundamentals, Overtones, and Combination Bands in Resonance Raman Spectra. *Inorg. Chem.* **1989**, *28*, 4358−4366.
(27) Sun, Z.; Lu, J.; Zhang, D. H.; Lee, S. Y. Quantum theory of (femtosecond) time-resolved stimulated Raman scattering. *J. Chem. Phys.* **2008**, *128*, 144114.
(28) Kukura, P.; McCamant, D. W.; Mathies, R. A. Femtosecond stimulated Raman spectroscopy. *Annu. Rev. Phys. Chem.* **2007**, *58*, 461−488.
(29) Quincy, T. J.; Barclay, M. S.; Caricato, M.; Elles, C. G. Probing Dynamics in Higher-Lying Electronic States with Resonance-Enhanced Femtosecond Stimulated Raman Spectroscopy. *J. Phys. Chem. A* **2018**, *122*, 8308−8319.
(30) McCamant, D. W.; Kukura, P.; Mathies, R. A. Femtosecond Broadband Stimulated Raman: A New Approach for High-Performance Vibrational Spectroscopy. *Appl. Spectrosc.* **2003**, *57*, 1317−1323.
(31) McCamant, D. W.; Kukura, P.; Yoon, S.; Mathies, R. A. Femtosecond broadband stimulated Raman spectroscopy: Apparatus and methods. *Rev. Sci. Instrum.* **2004**, *75*, 4971−4980.
(32) Prince, R. C.; Frontiera, R. R.; Potma, E. O. Stimulated Raman scattering: From bulk to nano. *Chem. Rev.* **2017**, *117*, 5070−5094.
(33) Pontecorvo, E.; Ferrante, C.; Elles, C. G.; Scopigno, T. Structural rearrangement accompanying the ultrafast electrocyclization reaction of a photochromic molecular switch. *J. Phys. Chem. B* **2014**, *118*, 6915−6921.
(34) Marangoni, M.; Brida, D.; Quintavalle, M.; Cirmi, G.; Pigozzo, F. M.; Manzoni, C.; Baronio, F.; Capobianco, A. D.; Cerullo, G. Narrow-bandwidth picosecond pulses by spectral compression of femtosecond pulses in a second- order nonlinear crystal. *Opt. Exp.* **2007**, *15*, 174−180.
(35) Pontecorvo, E.; Ferrante, C.; Elles, C. G.; Scopigno, T. Spectrally tailored narrowband pulses for femtosecond stimulated Raman spectroscopy in the range 330−750 nm. *Opt. Express* **2013**, *21*, 6866.
(36) Frisch, M. J.; Trucks, G. W.; Schlegel, H. B.; Scuseria, G. E.; Robb, M. A.; Cheeseman, J. R.; Montgomery, J. A., Jr.; Vreven, T.; Kudin, K. N.; Burant, J. C. et al. *Gaussian 03*, Revision D.01; 2004.
(37) Barclay, M. S.; Elles, C. G.; Caricato, M. On the Discrepancy between Experimental and Calculated Raman Intensities for Conjugated Phenyl and Thiophene Derivatives. *J. Phys. Chem. A* **2020**, *124*, 4678−4689.
(38) *NIST Computational Chemistry Comparison and Benchmark Database, NIST Standard Reference Database Number 101*. 2020; http://cccbdb.nist.gov/.
(39) Barclay, M. S.; Elles, C. G.; Caricato, M. Benchmark Study of Ground-State Raman Spectra in Conjugated Molecules. *J. Chem. Theory Comput.* **2020**, *16*, 612−620.
(40) Barclay, M. S.; Quincy, T. J.; Williams-Young, D. B.; Caricato, M.; Elles, C. G. Accurate Assignments of Excited-State Resonance Raman Spectra: A Benchmark Study Combining Experiment and Theory. *J. Phys. Chem. A* **2017**, *121*, 7937−7946.
(41) Green, D.; Roy, P.; Hall, C. R.; Iuliano, J. N.; Jones, G. A.; Lukacs, A.; Tonge, P. J.; Meech, S. R. Excited State Resonance Raman of Flavin Mononucleotide: Comparison of Theory and Experiment. *J. Phys. Chem. A* **2021**, *125*, 6171−6179.
(42) Batignani, G.; Pontecorvo, E.; Giovannetti, G.; Ferrante, C.; Fumero, G.; Scopigno, T. Electronic resonances in broadband stimulated Raman spectroscopy. *Sci. Rep.* **2016**, *6*, 1−8.
(43) Oscar, B. G.; Chen, C.; Liu, W.; Zhu, L.; Fang, C. Dynamic Raman Line Shapes on an Evolving Excited-State Landscape: Insights from Tunable Femtosecond Stimulated Raman Spectroscopy. *J. Phys. Chem. A* **2017**, *121*, 5428−5441.
(44) Boggio-Pasqua, M.; Ravaglia, M.; Bearpark, M. J.; Garavelli, M.; Robb, M. A. Can Diarylethene Photochromism be Explained by a Reaction Path Alone? A CASSCF Study with Model MMVB Dynamics. *J. Phys. Chem. A* **2003**, *107*, 11139−11152.
(45) Valley, D. T.; Hoffman, D. P.; Mathies, R. A. Reactive and unreactive pathways in a photochemical ring opening reaction from 2D femtosecond stimulated Raman. *Phys. Chem. Chem. Phys.* **2015**, *17*, 9231−9240.
(46) Sotome, H.; Une, K.; Nagasaka, T.; Kobatake, S.; Irie, M.; Miyasaka, H. A dominant factor of the cycloreversion reactivity of diarylethene derivatives as revealed by femtosecond time-resolved absorption spectroscopy. *J. Chem. Phys.* **2020**, *152*, 152.
(47) Trulson, M. O.; Dollinger, G. D.; Mathies, R. A. Excited state structure and femtosecond ring-opening dynamics of 1,3-cyclohexadiene from absolute resonance Raman intensities. *J. Chem. Phys.* **1989**, *90*, 4274−4281.
(48) Reid, P. J.; Doig, S. J.; Wickham, S. D.; Mathies, R. A.; Doig, S. J. Photochemical Ring-Opening Reactions Are Complete in Picoseconds: A Time-Resolved UV Resonance Raman Study of 1,3-Cyclohexadiene. *J. Am. Chem. Soc.* **1993**, *115*, 4754−4763.
(49) Trulson, M. O.; Dollinger, G. D.; Mathies, R. A. Femtosecond Photochemical Ring Opening Dynamics of Redetermination of the Experimental Electron Deformation Density of Benzenetricarbonylchromium. *J. Am. Chem. Soc.* **1987**, *109*, 586−587.
(50) Reid, P. J.; Lawless, M. K.; Wickham, S. D.; Mathies, R. A. Determination of Pericyclic Photochemical Reaction Dynamics with Resonance Raman Spectroscopy. *J. Phys. Chem.* **1994**, *98*, 5597−5606.
(51) Reid, P. J.; Doig, S. J.; Mathies, R. A. Direct measurement of the photochemical ring opening in 1,3-cyclohexadiene by picosecond time-resolved UV resonance Raman. *Chem. Phys. Lett.* **1989**, *156*, 163−168.
(52) Garavelli, M.; Page, C. S.; Celani, P.; Olivucci, M.; Schmid, W. E.; Trushin, S. A.; Fuss, W. Reaction path of a sub-200 fs photochemical electrocyclic reaction. *J. Phys. Chem. A* **2001**, *105*, 4458−4469.

https://doi.org/10.1021/acs.jpca.2c05435
J. Phys. Chem. A 2022, 126, 5932−5939